Neutral-Ionic State Correlations in Strong-Field Molecular Ionization

Marija Kotur, Congyi Zhou, Spiridoula Matsika, Serguei Patchkovskii, Michael Spanner, and Thomas C. Weinacht

Phys. Rev. Lett. **109**, 203007 — Published 14 November 2012

DOI: 10.1103/PhysRevLett.109.203007

Neutral-Ionic State Correlations in Strong-Field Molecular Ionization

Marija Kotur,[1] Congyi Zhou,[2] Spiridoula Matsika,[2] Serguei Patchkovskii,[3] Michael Spanner,[3] and Thomas C. Weinacht[1]

[1]*Department of Physics and Astronomy, Stony Brook University, Stony Brook, New York 11794 USA*
[2]*Department of Chemistry, Temple University, Philadelphia, PA 19122 USA*
[3]*Steacie Institute for Molecular Sciences, National Research Council of Canada, Ottawa, ON, Canada K1A 0R6*

We study correlations between neutral and ionic states in strong-field molecular ionization. We compare predictions based on Dyson orbital norms and quasi-static semiclassical tunneling theories (Keldysh and MO-ADK) with more detailed calculations of strong-field ionization which take into account i) the Coulomb interaction between the outgoing continuum electron wave packet and the remaining bound electrons and ii) electron-core interactions that cause distortions of the electronic continuum states during the ionization event. Our results highlight the prominence of electronic rearrangement effects in strong-field ionization with intense ultrafast laser pulses, where the outgoing continuum electron can cause electronic transitions in the parent ion. Calculations and measurements for excited uracil molecules reveal the breakdown of Keldysh-weighted Dyson norm predictions for ionization to different states of the molecular cation in the strong-field regime.

PACS numbers:

Strong-field ionization of molecules is at the forefront of ultrafast atomic, molecular and optical science [1–6]. It is a key ingredient in the initiation of attosecond electron dynamics [7, 8] and in the production of attosecond pulses in the soft x-ray region of the spectrum [9–12]. It is the first step in high-harmonic generation (HHG) spectroscopies [14, 15], and is also an important tool for probing molecular dynamics in time-resolved ionization measurements [13]. Finally, it is sensitive to, and can therefore serve as a probe of, electron correlation [16, 17].

While strong-field ionization of atoms and high harmonic generation received considerable attention in the late 1980s [18], there has been a resurgence of interest in strong-field *molecular* ionization in the past few years. Unlike weak-field photoionization, the description of the light matter interaction in the strong-field low-frequency regimes requires non-perturbative, typically timer-dependent approaches. To date, quasi-static tunneling theory [19–23] has been used as the basis for most popular models of molecular ionization [24–28]. While there has been much success in modeling the ionization of small (mostly diatomic) molecules, our understanding of multielectron dynamics in polyatomics is just developing [29]. The central theme of attosecond science is to measure electronic structure and dynamics in real-time, much as femtochemistry allowed direct measurement of nuclear dynamics on nuclear timescales. Multielectron dynamics are then of central importance in attosecond science and are expected to play an even more important role in larger molecules, where, for example, closely spaced ionic states allow for strong field ionization from multiple orbitals [30]. Many recent studies on strong-field and HHG spectroscopies cite the goal of measuring multielectron structure and dynamics in molecules as a motivating factor [14, 31–33]. However, these same studies typically use simple semiclassical and/or single-active-electron models to interpret the experimental measurements.

In this work we investigate the distribution of final ionic states after ionization - i.e. from which orbitals were electrons removed during ionization. Ionization is the first step in HHG, and a quantitative understanding of which cation states are accessed following ionization is crucial for a correct interpretation of the HHG spectra. Several recent papers (in addition to some work in the early 1990's) have addressed the issue of removing electrons from orbitals below the highest occupied molecular orbital (HOMO) [34–36]. While it has been established that ionization of more deeply bound electrons can occur in the strong field of an ultrafast laser pulse, there is currently no general understanding of which final states of the cation are populated, and with what probability. We compare three methods for predicting ionization to different ionic states of the molecular cation: Keldysh-weighted Dyson orbital norms, molecular ADK (MO-ADK) theory [26], and numerical calculations based on a time-dependent mixed orbital/grid-based method outlined in Ref. [37]. We apply the methods to calculate ionization yields from the three lowest singlet states of uracil to the lowest 8 doublet cation states. These calculations are compared with experiments on strong-field ionization of pre-excited uracil. Experimental measurements are in closer agreement with the detailed numerical computations and disagree with predictions based on Dyson orbital norms and quasi-static tunneling. These results expose a central weakness in standard models being applied to molecular strong-field ionization, and point to theoretical challenges that need to be addressed if attosecond science and HHG spectroscopies are to live up to the promise of measuring electronic structure and dynamics.

Koopmans' correlations [38], used in several recent studies [13, 39], are a simple way of predicting the fi-

nal state of an ionization process. They are based on Hartree-Fock theory, where only one electronic configuration is considered for each of the neutral or ionic states involved. The validity of the frozen orbital approximation is assumed as well, where ionic one-electron orbitals do not differ from their neutral counterparts, so that ionization is viewed as a removal of an electron from a single orbital, without any changes to the rest of the molecule. As Hartree-Fock theory does not capture the true multi-electron nature of the molecular wave function, and the frozen orbital approximation is frequently not valid, Koopmans' correlations can fail, even in the simplest case of weak field ionization.

In order to improve upon Koopmans' correlations in predicting final ionic state distributions, one can calculate a set of Dyson orbital magnitudes associated with the accessible ionization channels. Dyson orbitals are one-electron orbitals obtained by projecting a final ionic ($N-1$ electron) state, ψ_n (the n^{th} ionic state), onto the initial (N electron) neutral state, ψ_m: $|\psi_{Dyson}\rangle = \sqrt{N}\langle\psi_m^N(r_1, r_2, ..., r_N)|\psi_n^{N-1}(r_1, ..., r_{N-1})\rangle$. Since $|\psi_m^N\rangle$ and $|\psi_n^{N-1}\rangle$ are multielectron eigenstates of the neutral and the ionic Hamiltonians, both contributions from multiple configurations and orbital relaxation are taken into account. In the limit of weak field ionization, it can be shown that the probability of ionizing to a given ionic state from an initial neutral state is proportional to the corresponding Dyson orbital amplitude [40]. In the case of strong-field ionization, the simplest approximation yields a probability of ionizing to a particular ionic state given by the product of the Dyson orbital magnitude and the Keldysh tunneling exponent [21] associated with the ionization channel.

In order to account for electron rearrangement that may happen during the ionization process, we turn to calculations of strong-field ionization yields that go beyond the standard strong field approximation. The calculations, described below, utilize a more detailed description of the outgoing electron's interaction with the remaining cation. Our numerical multielectron strong-field ionization calculations, referred to as the time-dependent resolution-in-ionic states (TD-RIS) method, are carried out using the mixed orbital/grid-based formalism outlined in Ref. [37]. Further details are provided in the supplementary material.

We use a Ti:sapph laser (1 mJ, 1 kHz, 30 fs, 785 nm) in conjunction with a Mach-Zender interferometer and a time-of-flight mass spectrometer (TOFMS) to perform pump-probe measurements of dissociative ionization yields. Gas-phase uracil molecules are obtained by sublimation of powdered uracil at $\sim 140°$C, which was admitted into the vacuum chamber as an effusive molecular beam. They are excited ($S_0 \longrightarrow S_2$ transition) by 'pump' pulses with a central wavelength of 262 nm pulses ($h\nu_{pump}$=4.73 eV), having a pulse duration of about 50 fs, which are generated by frequency tripling of the laser output. The molecules are then probed by the intense pulses with a central wavelength of 785 nm ($h\nu_{probe}$=1.58 eV). The intensities of the UV pulses were $2-4$ TW/cm^2, with the IR pulses ranging between $7-100$ TW/cm^2. The Keldysh parameter associated with ionization from S_2 to low lying states of the molecular cation was between 0.7 and 1.2 for the probe intensities we used in our measurements. The experiments are thus carried out in a regime in which the ionization cannot be described in terms of either tunnel or multiphoton ionization alone. For more details see [55]. Figure 1 illustrates the experimental pump probe scheme and shows the relevant neutral and ionic states.

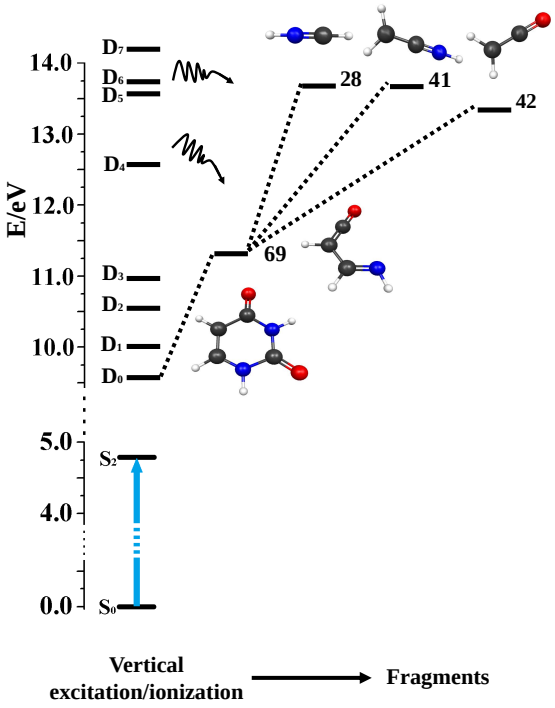

FIG. 1: Energies of the relevant neutral and ionic states, along with the dissociation energies/barriers to dissociation for the formation of prominent fragments in the TOFMS, measured from the vertical ionization point. As indicated by the blue arrow, the pump pulse excites the molecules from S_0 to the first bright state, S_2 after which the probe pulse ionizes the molecules to low lying states of the molecular cation, which can dissociate to form the fragments shown to the right hand side of the figure. The experimental energy for S_2 is shown while for the ionic states calculated values are shown.

Ab initio electronic structure calculations, shown in Fig.1, allow us to associate molecules ionized to a particular cationic state with fragments in the TOFMS. The left side of the figure shows the energies, measured from the vertical ionization point, of the first several ionic states. The right side of the figure shows the energy required to produce prominent fragments in the TOFMS (either the barrier to dissociation or the energy of the fragments - whichever is higher). A molecule with a total energy

above the dissociation threshold for a given fragment will dissociate to form the smallest fragments energetically allowed [56]. The production of fragment 69 requires about 2 eV of energy above the D_0 minimum, so without any internal vibrational energy, the molecule has to be ionized to D_4 or higher to produce this fragment. If the molecule acquires some vibrational kinetic energy in moving away from the Franck Condon (FC) region on S_2, or the molecule has some energy stored in other degrees of freedom, then ionization to states with energies below the fragment 69 dissociation threshold can lead to the detection of 69 in the TOFMS.

To determine which ionic states below D_4 can produce the 69 amu fragment, we considered the vibrational energy the molecule can acquire through relaxation on the S_2 potential, as well as the thermal energy stored in the molecules at the operational temperature. Relaxation from the FC region to the S_2 minimum is accompanied by a gain of up to 0.5 eV in vibrational kinetic energy [57, 58]. Based on dissociative ionization measurements of room temperature halogenated methanes, which found dissociated fragments for excitation energies up to about 0.15 eV below the dissociation energy [56], we estimate that there is about ∼0.6-0.7 eV of energy in other degrees of vibrational freedom which is available for dissociation . This estimate is based on multiplying 0.15 eV by the ratio of the number of degrees of vibrational freedom in the two molecules (30/9) and the ratio of the molecular temperatures (440K/300K). Given the calculated dissociation barriers, fragment energies, relaxation on S_2, and the internal energy stored in the molecule, we conclude that ionization to states D_2 - D_4 will lead to the production of fragment 69 in the TOFMS. Since the total energy available for dissociation on a given ionic state may vary with time delay, and involves the pooling of energy from multiple degrees of freedom, we also consider how sensitive our interpretation is to which states dissociate to form 69.

Molecules with energies greater than 4 eV above the D_0 minimum can fragment further to produce fragments 42, 41 and 28 [51, 59]. Thus depositing 4 eV or more of energy into the molecule leads to Dyson-allowed states, but with enough energy to dissociate into fragments lighter than 69, making 69 the signature of Dyson-forbidden ionization from S_2. Since the calculations only provide relative yields, the most sensitive probe of the calculations at our disposal is the change in 69/112 in going from S_0 to S_2. Thus by looking at how the 69 yield (normalized to the parent to account for changes in the IP associated with going from S_0 to S_2) changes with time delay (i.e. ionizing from S_0 for negative delays and S_2 for positive delays) we can test the Dyson norm predictions for ionization from S_2.

Figure 3 shows the comparison of the state-resolved, strong-field ionization yields calculated using (i) Dyson orbital norms weighted by the Keldysh tunneling exponent, $|\langle\psi_{Dyson}|\psi_{Dyson}\rangle|\exp[-(2/3)(2I_p)^{3/2}/F_0]$, where I_p is the ionization potential and F_0 is the peak electric field strength [61], (ii) the MO-ADK method [26], and the TD-RIS method. Calculations have been carried out for ionization from the ground state, S_0, of the neutral (left column), and the first bright excited neutral state, S_2 (right panel). Calculations were carried out for the ground state (S_0) equilibrium geometry. For simplicity, the results of each calculation shown in Fig.3 have been normalized to make the maximum ionization yield unity, thus focusing on the relative yields.

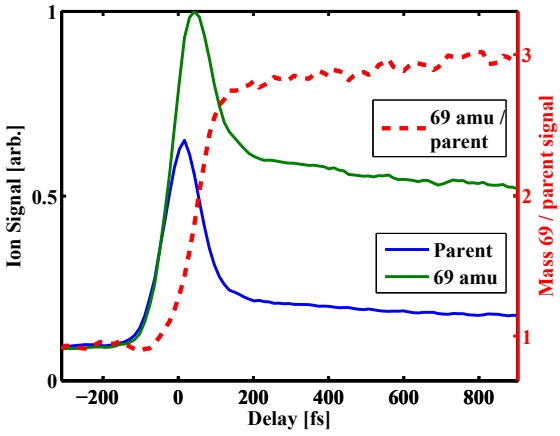

FIG. 2: Pump-probe ion signals for the parent (blue solid line) and 69 amu (green solid line), and their ratio (red dashed line)

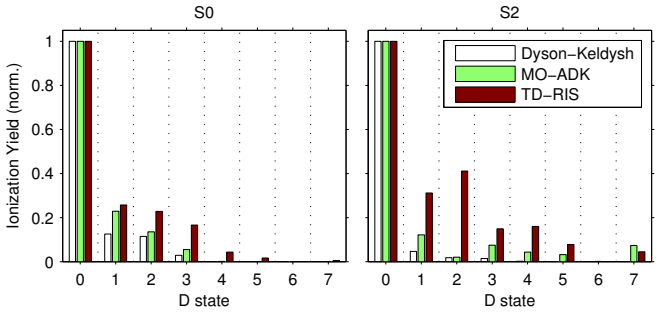

FIG. 3: Comparison of Dyson-Keldysh, MO-ADK, and TD-RIS calculations for ionization to the various doublet cation states of uracil starting from the ground state (S_0) and first bright excited state of the neutral molecule (S_2).

In uracil, the low lying states of both the neutral and the cation have a single dominant configuration, which allows us to describe the ionic states in terms of in terms of orbitals that are singly occupied. The first five ionic states (D_0-D_4) correspond to removal of an electron from a single orbital, leaving one singly occupied orbital ('single hole' states). Thus, they have large Dyson amplitudes from the neutral ground state (S_0). In contrast, the excited states S_1 and S_2, have configurations where an electron is moved from the HOMO or HOMO-1 to the LUMO (Lowest Unoccupied Molecular Orbital). Conse-

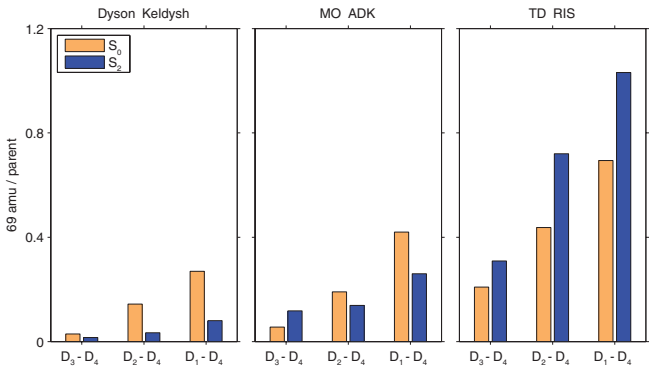

FIG. 4: Predicted 69/112 ratios for positive (S_2) and negative (S_0) time delays for the TD-RIS calculations and ADK weighted Dyson orbital amplitudes considering different combinations of ionic states leading to fragment 69.

quently they are only Dyson-correlated with one ionic state that has one singly occupied orbital. If we consider S_2, which corresponds to a HOMO→LUMO excitation, removal of the LUMO electron will leave the molecule in the ground state of the ion, which has a single hole in the HOMO orbital. The removal of any other electron leads either to a state with three unpaired electrons or a highly excited state with a double hole in the HOMO. The lowest states above D_0 which are Dyson-correlated with S_2 are D_5 and D_6, each of which has three unpaired electrons. We thus look for ionization to states D_2 - D_4 in order to test for breakdown of Dyson-weighted tunneling predictions. We focus on short pump-probe delays, at which the S_1 state is not yet populated (via non-adiabatic coupling between S_2 and S_1), and essentially all excited population is in S_2.

As Fig. 4 illustrates, the three calculational methods give very different predictions for the ratio of 69/112 starting from S_0 or S_2 (corresponding to pre- and post-excitation pump-probe delays). The Dyson-Keldysh estimate predicts a decrease in the 69/112 ratio in going from S_0 to S_2, whereas the TD-RIS calculation results predict an increase, regardless of whether molecules can dissociate to form 69 starting from D_1, D_2 or D_3. Whether the MO-ADK predicts an increase or decrease depends on which cation states are assumed to yield a 69 fragment. The TD-RIS computations consistently give the largest 69/parent ratio of all three methods regardless of which states are assumed to form the 69 fragment. Fig. 2 shows the measured ion yields for the 69 amu fragment and the parent ion, as well as their ratio as a function of pump-probe time delay. The measurements of the time dependence of the ratio, which show an increase in the ratio upon excitation of the S_2 state, are in closest qualitative agreement with the TD-RIS calculations, but disagree with the Dyson-Keldysh and MO-ADK predictions which do not uniformly predict an increase in the 69/parent ratio. While the calculations agree with the measurements in predicting an increase in the 69/112 ratio as a function of time delay, the calculations generally predict a smaller ratio for both positive and negative delays than found in the measurements. This may be due to multiple factors, including the fact that the calculations do not include laser driven coupling between different ionic states, which may be important in cases where there is a resonance between D_0 and a higher lying ionic state (such as D_3 for uracil, which is about 1.6 eV above D_0) [60]. Although none of the calculation methods predict a 69/parent ratio ratio as large as seen experimentally, the TD-RIS shows the largest predicted ratio and hence is again in best qualitative agreement with experiment.

We demonstrate the breakdown of Keldysh-weighted Dyson norms in predicting final state distributions for strong field ionization of a polyatomic molecule. The TD-RIS method, which utilizes a more detailed treatment of the electron-ion interaction gives ionization yields to different electronic states of the cation that are in best qualitative agreement with our strong-field ionization measurements. These results emphasis the need for theoretical tools to go beyond the traditional quasi-static semiclassical methods, successful in treating strong-field problems for atoms and small molecules, as strong-field techniques are applied to polyatomic molecules.

We gratefully acknowledge the support from the Department of Energy under award numbers DE-FG02 − 08ER15983 and DE-FG02 − 08ER15984.

[1] Z. Chang and P. Corkum, J. Opt. Soc. Am. B **27**, B9 (2010).
[2] T. Popmintchev *et al.*, Nature Photonics **4**, 822 (2010).
[3] U. Keller, IEEE Photonics Journal **2**, 225 (2010).
[4] K. Midorikawa, Y. Nabekawa, and A. Suda, Progress in Quantum Electronics **32**, 43 (2008).
[5] P. Agostini and L. DiMauro, Rep. Prog. Phys. **67**, 813 (2004).
[6] F. H. M. Faisal, Theor. Chim. Acta **127**, 175 (2010).
[7] E. Goulielmakis *et al.*, Nature **466**, 739 (2010).
[8] A. Fleischer *et al.*, Phys. Rev. Lett. **107**, 113003 (2011).
[9] F. Krausz and M. Ivanov, Rev. Mod. Phys. **81**, 163 (2009).
[10] M. Nisoli and G. Sansone, Progress in Quantum Electronics **33**, 17 (2009), ISSN 0079-6727.
[11] P. Corkum and F. Krausz, Nature Physics **3**, 381 (2007).
[12] M. F. Kling and M. J. J. Vrakking, Annu. Rev. Phys. Chem. **59**, 463 (2008).
[13] W. Li *et al.*, Proc. Natl. Acad. Sci. USA **107**, 20219 (2010).
[14] H.J. Wörner *et al.*, Nature **466**, 604 (2010).
[15] H.J. Wörner *et al.*, Science **334**, 208-212 (2011).
[16] C. F. de Morisson Faria and X. Liu, Journal of Modern Optics **58**, 1076 (2011).
[17] J. Breidbach and L. S. Cederbaum, Phys. Rev. Lett. **94**, 033901 (2005).
[18] B. Sheehy and L. F. DiMauro, Ann. Rev. Phys. Chem. **47**, 463 (1996).
[19] M. V. Ammosov, N. B. Delone, and V. P. Krainov, Sov. Phys.–JETP **64**, 1191 (1986).
[20] A. Perelomov, V. Popov, and M. Terentev, Sov. Phys. JETP **23**, 924 (1966).
[21] L. V. Keldysh, Sov. Phys. JETP **20**, 1307 (1965).
[22] F. H. M. Faisal, J. Phys. B. **6**, L89 (1973).
[23] H. R. Reiss, Phys. Rev. A **22**, 1786 (1980).
[24] M. DeWitt and R. Levis, J. Chem. Phys. **110**, 11368 (1999).
[25] X. M. Tong, Z. X. Zhao, and C. D. Lin, Phys. Rev. A **66**, 033402 (2002).
[26] K. Mishima *et al.*, Phys. Rev. A **70**, 063414 (2004).
[27] T. Brabec *et al.*, Phys. Rev. Lett. **95**, 073001 (2005).
[28] A. N. Markevitch *et al.*, Phys. Rev. A **69**, 013401 (2004).
[29] A.E. Boguslavskiy *et al.*, Science **335**, 1336 (2012).
[30] O. Smirnova *et al.*, Proc. Natl. Acad. Sci. USA **106**, 16556 (2009).
[31] C. Vozzi *et al.*, Nature Physics **7**, 822 (2011).
[32] L. Holmegaard *et al.*, Nature Physics **6**, 428 (2010).
[33] C.I. Blaga *et al.*, Nature **483**, 194 (2012).
[34] G. N. Gibson *et al.*, Phys. Rev. Lett. **67**, 1230 (1991).
[35] H. Akagi et al., Science **325**, 1364 (2009).
[36] B. K. McFarland *et al.*, Science **322**, 1232 (2008).
[37] M. Spanner and S. Patchkovskii, Phys. Rev. A **80**, 063411 (2009).
[38] T. Koopmans, Physica **1**, 104 (1934).
[39] V. Blanchet *et al.*, Nature (London) **401**, 52 (1999).
[40] B. Pickup, Chemical Physics **19**, 193 (1977).
[41] T. Otobe, K. Yabana, and J.-I. Iwata, Phys. Rev. A **69**, 053404 (2004).
[42] M. W. Schmidt *et al.*, J. Comput. Chem. **14**, 1347 (1993).
[43] J. Muth-Böhm, A. Becker, and F. H. M. Faisal, Phys. Rev. Lett. **85**, 2280 (2000).
[44] Z. Walters and O. Smirnova, J. Phys. B **43**, 161002 (2010).
[45] D. E. Manolopoulos, J. Chem. Phys. **117**, 9552 (2002).
[46] V. I. Lebedev, USSR Comp. Math, and Math. Phys. **15**, 44 (1975).
[47] H. Nakano, J. Chem. Phys. **99**, 7983 (1993).
[48] H. Nakano, Chem.Phys.Lett. **207**, 372 (1993).
[49] S. Matsika *et al.*, Discuss. Faraday Soc. **153**, 247 (2011).
[50] K. Raghavachari *et al.*, Chem. Phys. Lett. **157**, 479 (1989).
[51] C. Zhou *et al.*, J. Phys. Chem. A (submitted) (2011).
[52] M. J. Frisch *et al.*, et al., *Gaussian 03, revision c.02* (2004), gaussian, Inc., Wallingford, CT, 2004.
[53] M. Valiev *et al.*, Comput. Phys. Commun. **181**, 1477 (2010).
[54] B.M.Bode and M.S.Gordon, J. Mol. Graphics Mod.. **16**, 133 (1998).
[55] M. Kotur *et al.*, J. Chem. Phys. **134**, 184309 (2011).
[56] A. F. Lago *et al.*, J. Phys. Chem. A **109**, 1802 (2005).
[57] S. Matsika, The Journal of Physical Chemistry A **108**, 7584 (2004).
[58] H. R. Hudock *et al.*, The Journal of Physical Chemistry A **111**, 8500 (2007).
[59] M. Kotur *et al.*, Phys. Rev. X 021010 (2011).
[60] D. Cardoza, B. J. Pearson, and T. C. Weinacht, J. Chem. Phys. **126**, 084308 (2007).
[61] The Dyson norms (not weighted by the Keldysh exponent) for S_0 to D_0-D_7 are 0.87, 0.74, 0.83, 0.74, 0.71, 0.57, 0.00, 0.04 respectively. For S_2 they are 0.46 0.05 0.02, 0.04 0.07 0.11, 0.00, 0.48.